IEEE Access
Multidisciplinary ⋮ Rapid Review ⋮ Open Access Journal

Received May 17, 2022, accepted June 13, 2022, date of publication June 16, 2022, date of current version June 22, 2022.

Digital Object Identifier 10.1109/ACCESS.2022.3183745

The Sardinia Space Communication Asset: Performance of the Sardinia Deep Space Antenna X-Band Downlink Capability

GIUSEPPE VALENTE[1], MARIA NOEMI IACOLINA[1], RICCARDO GHIANI[2], ANDREA SABA[1], GIAMPAOLO SERRA[1], ENRICO URRU[1], GIORGIO MONTISCI[2], (Senior Member, IEEE), SARA MULAS[1,3], SAMI W. ASMAR[4], TIMOTHY T. PHAM[4], JAVIER DE VICENTE[5], AND SALVATORE VIVIANO[1]

[1]Italian Space Agency (ASI), 00133 Rome, Italy
[2]Dipartimento di Ingegneria Elettrica ed Elettronica, Università degli Studi di Cagliari, 09123 Cagliari, Italy
[3]Dipartimento di Fisica, Università degli Studi di Cagliari, 09042 Monserrato, Italy
[4]NASA's Jet Propulsion Laboratory, California Institute of Technology, Pasadena, CA 91109, USA
[5]ESA-ESOC, 64293 Darmstadt, Germany

Corresponding author: Giuseppe Valente (giuseppe.valente@asi.it)

ABSTRACT The Sardinia deep space antenna (SDSA), managed by the Italian Space Agency (ASI) has started its operations in 2017 aiming to provide tracking and communication services for deep space, near earth, and lunar missions, and to support new and challenging radio science experiments. The SDSA shares with the Sardinia Radio Telescope (SRT) a part of the system and infrastructure, but has its own specific equipment and a dedicated control center. The current SDSA capabilities involve the X-band (8.4 GHz–8.5 GHz) reception of telemetry from deep space probes within interplanetary missions. In this work we describe the development and performance of the X-band receiving system. It was designed and assembled with the cooperation of both the NASA-Jet Propulsion Laboratory (JPL) and the European Space Agency (ESA). Specifically, NASA-JPL provided the X-band feed and the cryogenic receiver installed in a suitable focus of the SRT devoted to space applications, and ESA provided the intermediate frequency modem system (IFMS) for signal processing. The coupling of the X-band feed with the parabolic reflector of the SRT and the radiating features of the SDSA have been evaluated with simulations performed using CST Studio Suite and GRASP by Ticra. The telecommunication performance of the system has been assessed by measurements and experiments showing a good agreement between estimates and simulations.

INDEX TERMS Antennas, deep space network, receivers, reflector antennas.

I. INTRODUCTION

The Sardinia Radio Telescope (SRT) (Fig. 1) is a general-purpose fully steerable 64-meter diameter radio telescope operating with high efficiency across the 0.3-116 GHz frequency range [1], [2] and designed to be used for astronomy [2]–[5], geodesy, and space science [6], [7].

The SRT is managed by the Italian National Institute for Astrophysics (INAF) for radio astronomy purposes and partially funded by ASI, which employs it for deep space tracking and communications. The infrastructure, the equipment, and the operations relevant to the deep space communication (DSC) and tracking activities, performed at SRT site under ASI's responsibility, constitute the Sardinia space asset, also known as Sardinia Deep Space Antenna (SDSA).

In the following we will refer to SRT when describing the general antenna characteristics and to SDSA when dealing with the antenna features within the ASI space assets.

The telescope is located 35 km North of Cagliari (Italy) in the Mediterranean island of Sardinia at about 600 m above the sea level. The optical design is based on a quasi-Gregorian configuration (Fig. 1) with a shaped 64-meter diameter primary reflector (M1) and a 7.9-meter diameter secondary reflector (M2). The rotating mirror M3 and the fixed mirrors M4 and M5 are part of the so-called beam waveguide (BWG) system (see Fig. 2). Specifically, M3 and M5 are currently devoted to the SDSA initial operational capabilities (IOC),

The associate editor coordinating the review of this manuscript and approving it for publication was Kwok L. Chung.

FIGURE 1. The sardinia radio telescope.

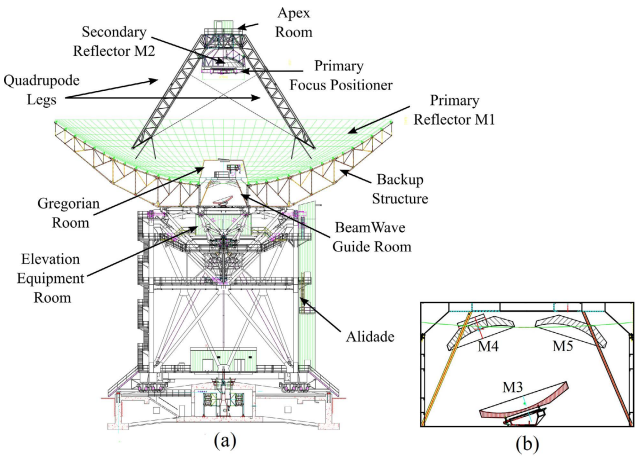

FIGURE 2. Sketch of the sardinia radio telescope (a) and detail of the BWG room (b).

i.e. the BWG optical configuration, enabling the downlink of spacecraft signals at X-frequency band.

The SRT is equipped with an active remote controlled optics, composed of an active surface mounted on the M1 backup structure and six electro-mechanical actuators installed behind M2. The M1 active surface consists of 1008 aluminum panels (with a panel manufacturing root-mean-square error (RMSE) less than 70 μm) and 1116 electromechanical actuators, able to compensate the gravitational deformation of the backup structure. The M2 actuators provide six degrees of freedom for an accurate monitoring and control of the sub-reflector position. The primary reflector surface was aligned with an accuracy below 300 μm RMS at 45° elevation by photogrammetry measurements [1]. Then, combined photogrammetric and laser tracker measurements in the elevation range 15°-90° provided the input to two look-up tables for the M1 active surface actuators and for the M2 actuators, respectively. These information are employed to correct both the M1 surface deformations and the M1/M2 axes misalignment as a function of the antenna elevation angle.

The SDSA facilities allow ASI to join the worldwide DSC network dedicated to data acquisition from deep space missions. In the near future, the SDSA is expected to provide a DSC service to the NASA deep space network (DSN) [8] and to the ESA tracking station network (ESTRACK) [9], but also to operate as a stand-alone infrastructure for other space applications.

A feasibility study of a new optical configuration is ongoing to equip the SDSA with a full operational capability (FOC). This perspective would enhance the current SDSA functionality with a new telemetry, tracking and command (TT&C) asset for both deep space and near earth missions at X- as well as K- and Ka- frequency bands allocated to the space research. Also, the SDSA FOC could ensure emergency operations or provide a strategic backup when redundancy is required, as in the case of space missions with high scientific relevance or subjected to potential critical issues.

Moreover, the cooperation between ASI and INAF will enable the SDSA to cover several frequency bands otherwise not available in other facilities of the DSN and ESTRACK, such as, e.g., the P band [5], allowing the tracking of the entry, descent and landing (EDL) phases of space rovers, by processing the information given by the doppler shift of the UHF carrier [10]. Indeed, the current SRT configuration can host up to twenty receivers, which can be installed in four different focal positions: the primary focus (F1) with focal length to diameter ratio (F/D) equal to 0.33, the Gregorian focus (F2) with F/D equal to 2.34, and the BWG foci F3 and F4 with F/D 1.38 and 2.81, respectively [11]. Thanks to the possibility of exploiting the large number of operating frequency bands of the SRT, the SDSA will also be able to investigate new technological and operative solutions.

The SDSA activity has been started recently thanks to a specific agreement of ASI with NASA, aiming to future collaboration within forthcoming interplanetary missions. Technical and operative support provided by the NASA-Jet Propulsion Laboratory (JPL) helped to start the development of the SDSA functionalities. Partnership with ESA enabled the installation of the intermediate frequency modem system (IFMS) backend into the shielded room of SRT, which has allowed SDSA operators to acquire and record the signal from spacecrafts.

The aim of this work is to describe the set up and the performance of the new X-band Sardinia space communication asset. In Section II, we describe the development, the optical configuration, and the architecture of the current SDSA IOC, i.e. the first step towards the full operational capability of the Sardinia space communication asset. In Sections III and IV, the radiating features and the downlink performance of the

SDSA have been deeply investigated. Simulations have been performed using the commercial software CST Studio Suite and GRASP by Ticra, whereas the experimental validation is provided by observation of known calibrator radio sources. Then, in Section V, the antenna sensitivity has been validated by processing the signal acquired during tracking sessions of the NASA Juno Mission [12]. Finally, conclusion and future perspective are discussed.

II. SDSA X-BAND CONFIGURATION

The present configuration of the SDSA operates in the frequency range 8.4-8.5 GHz, which is the fraction of the X-band allocated to the space research service by the International Telecommunication Union (ITU) for the use in deep space and near-earth communications. The near-earth band, between 8.45 GHz and 8.50 GHz, is used for the reception of signals from space probes at less than 2,000,000 km from Earth [13], whereas the deep space band, between 8.40 GHz and 8.45 GHz, is used for the downlink from space probes at more than 2,000,000 km from Earth [13].

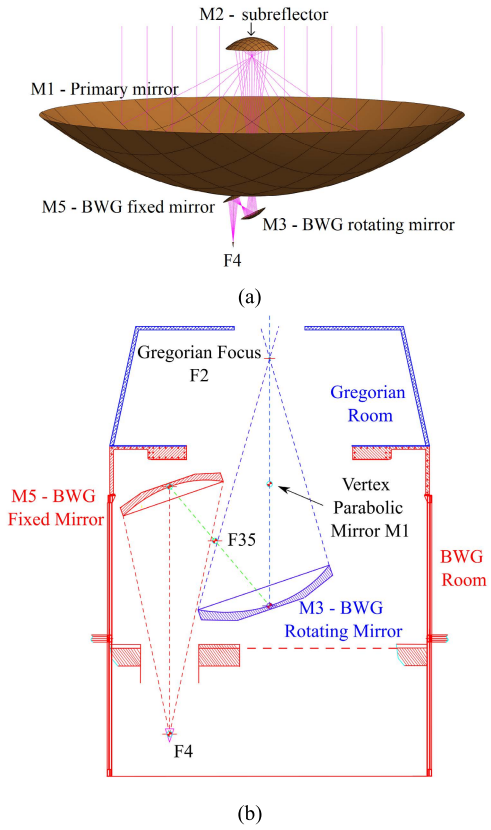

FIGURE 3. Optical configuration of the SDSA in the X-band (GRASP model) (a), and detail of the mirrors in the BWG room (mirror M4 is not shown) (b). F35 is the common focus of mirrors M3 and M5.

The optical configuration of the SDSA in the X-band is shown in Fig. 3. It is composed of the primary mirror M1, the axially symmetric sub-reflector M2, the rotating mirror M3, and the fixed mirror M5. Mirrors M3 and M5 are portions of ellipsoids with major axis a and minor axis b (see table 1). The focus of the mirror M5 is the focal position F4 of the SRT, where the feed horn devoted to space operations is housed. In table 1 the geometrical parameters of the mirrors are listed.

The optimum theoretical value of the M5 aperture illumination taper is -12 dB at $\pm 10°$ (see Fig. 3b).

TABLE 1. Size of the SRT mirrors employed for deep space communication.

Mirror	Size	*a*	*b*	*F/D*
M1	64 m (axially symmetrical)	-	-	0.33
M2	7.9 m (axially symmetrical)	-	-	2.34
M3	3.921 m × 3.702 m	4.7 m	3.8516 m	-
M5	2.994 m × 2.823 m	4.5 m	3.516 m	2.81

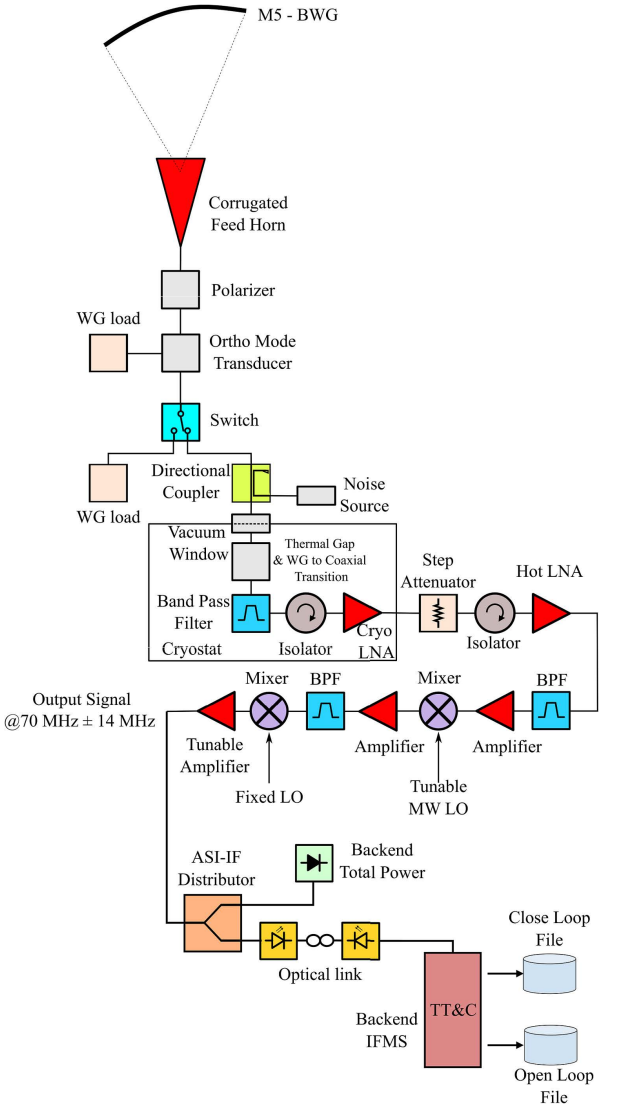

FIGURE 4. Block diagram of the X-band receiver (front end and down conversion section) borrowed from JPL-NASA and IFMS borrowed from ESA.

The whole receiving system is represented in Fig. 4, which also depicts the measurement setup, composed of the backend total power and the IFMS backend.

A X-band cryogenic receiver borrowed from JPL-NASA was installed in F4 (see Fig. 4) with a RF bandwidth of 700 MHz centered at 8.45 GHz. Basically, it consists of a corrugated circular feed horn (see [14]) providing the required illumination for M5, a waveguide polarizer and an orthomode transducer providing right-hand circular polarization (RHCP) or left-hand circular polarization (LHCP), and a cryostat hosting the cryogenic LNA that operates at the physical temperature of 10 K. A down conversion section amplifies, filters, and converts the RF band (8.1 GHz–8.8 GHz) down to the intermediate frequency (IF) band (70 MHz ± 14 MHz). Then, the 70 MHz right-hand or left-hand circular polarized signal can be processed, after an IF distributor (ASI-IF distributor in Fig. 4), either using a total power backend or using a dedicated backend for space applications, named Intermediate Frequency Modem System (IFMS), borrowed from ESA [15]. The total power section is used to calibrate the system, whereas the IFMS operates both in close loop mode (mainly for demodulation and decoding) and in open loop mode. The latter allows to acquire the baseband in-phase and quadrature (IQ) data of the received signal for post-processing. The baseband signal (which is divided into 4 sub-bands/channels of equal size) is recorded into binary files that contain all the available information (i.e., sample rate, quantization, frequency, sample time tags, gain configuration, and so on) aiming to reconstruct the detected signal. Then, from the IFMS output, the IQ data can be used for different types of signal processing, such as fast Fourier transform (FFT) or Doppler shift calculation.

III. RADIATING FEATURES OF THE SYSTEM

A detailed description of the X-band feed horn is available in [14], whereas the coupling between this feed and the SRT BWG optical configuration has been modeled and evaluated using the commercial software GRASP by Ticra. GRASP is a reliable tool for the analysis and design of reflector antenna systems that employs a physical optics (PO) algorithm as the baseline analysis method, supported by Moment Method (MoM) and Geometrical Theory of Diffraction (GTD) solvers for advanced applications.

First, we have modeled and simulated the feed [14] using CST Studio Suite: the simulated radiation pattern in the principal planes at 8.45 GHz is reported in Fig. 5 and the main results of the CST simulation are reported in Table 2. The edge taper at ±10° is −12 dB as required.

Then, the CST-simulated far field pattern has been imported as input of the GRASP project (see Fig. 3a) to evaluate the SDSA radiation performance.

Let D the actual antenna directivity and D_M the maximum directivity of the aperture [16], defined as:

$$D_M = \left(\frac{2\pi R_A}{\lambda}\right)^2 \tag{1}$$

wherein R_A is the radius of the M1 reflector aperture and λ is the free space wavelength. In our case $D_M = 75.07$ dBi. Then, the aperture efficiency η_A is defined as $D = \eta_A D_M$ and

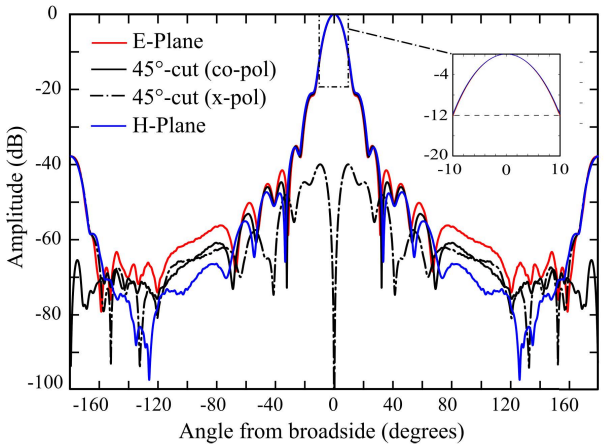

FIGURE 5. Simulated (CST Studio Suite) normalized far field pattern of the X-band feed horn. X-pol in the E-and H-plane are not shown since lower than −100 dB.

TABLE 2. Results of the CST simulations of the feed.

	Level/Source	Value
Frequency	System design	8.45 GHz
Simulation Mode	CST project	Time Domain
Feed gain	CST simulations	25.3 dB
Edge taper at ±10°	CST simulations	-12 dB
HPBW	CST simulations	10.4°
SLL	CST simulations	-22 dB
Cross-polarization	CST simulations	< -40 dB

the antenna gain is:

$$G = \eta_A\, \eta_S\, \eta_B\, \eta_{RMS}\, \eta_{AM}\, \eta_O\, D_M = \eta D_M \tag{2}$$

wherein η is the overall efficiency and

i) η_S is the spillover efficiency;
ii) η_B is the blockage efficiency, including the effect of both the sub-reflector M2 and the quadrupods (Fig. 1);
iii) η_{RMS} is the Ruze RMS efficiency due to the manufacturing RMSE of mirrors M1, M2, M3, and M5; and to the alignment RMSE of M1 and M2 panels and active surface (see Table 3).
iv) η_{AM} accounts for the misalignment of the optical path in the BWG.
v) η_O represents the return loss efficiency, the ohmic efficiency, and the cross-polarization efficiency.

Using the GRASP model in Fig. 3a we have computed the aperture efficiency η_A, equal to 0.775.

The spillover efficiency has been computed enabling a dedicated GRASP subroutine, providing $\eta_S = 0.909$.

Then, the GRASP project has been modified including the quadrupods (not shown in Fig. 3a) and the blockage of the sub-reflector M2 to compute the blockage efficiency. The result of this simulation is $\eta_B = 0.907$.

The Ruze RMS efficiency is 0.97, computed using the Ruze equation [17] considering a total RMS surface error

TABLE 3. Estimated RMSE contributions to Ruze RMS efficiency.

Error source	RMSE (μm)
M1 panel manufacturing	70
M1 panel alignment	300
M1 back up structure and actuators	50
M2 panel manufacturing	50
M2 panel alignment	60
M2 back up structure and actuators	20
M3 manufacturing	230
M5 manufacturing	240
Total surface error	**463**

equal to 463 μm (see Table 3) and a wavelength equal to 355 mm at 8.45 GHz.

The η_O has been estimated at about 0.99.

Finally, we estimated a η_{AM} equal to 0.92. This value accounts for a residual misalignment of the BWG optics (M3-M5 coupling) that we are currently investigating to optimize the system performance.

As a result, the simulated overall efficiency η is 0.56 and the gain G is 72.4 dBi at 8.45 GHz. This value can be considered the best SDSA performance as the angular elevation changes.

In Table 4 we summarize the main radiating parameters resulting from the simulation of the SDSA GRASP project. In addition, in fig. 6 we compare the simulated and measured beam pattern of the SDSA. In fig. 6 the E-plane, H-plane, and 45°-cuts of the simulated far-field pattern virtually overlap and have been obtained with all the mirrors aligned according to the SRT optical design.

TABLE 4. Estimated radiation performance of the SDSA.

	Level	Value
Frequency	System design	8.45 GHz
Simulation Mode	GRASP project	physical optics
Efficiency (η)	GRASP simulations	0.56
Gain (G)	GRASP simulations	72.4 dB
HPBW	GRASP simulations	0.039°
SLL	GRASP simulations	-23 dB
Cross-polarization	GRASP simulations	< -40dB

A dedicated experiment was carried out on March 23rd 2021 to measure two orthogonal cuts of the SDSA far-field pattern at 8.45 GHz and compare them with the GRASP simulation (see Fig. 6). Such experiment consisted in moving the antenna along two orthogonal scans (also known as cross-scan mode) centered on the radio source calibrator 3C84, which is a strong variable flux radio source suitable for beam pattern measures that allows to highlight the sidelobe level (SLL) and their features [18]. Both scans were performed around the elevation angle of 66° since, as we will show in the next section (see Fig. 10), the optimal performance in the X-band of the SDSA, with the current optics configuration, is achieved between 60° and 80°. An integration time of 40 ms was set in the total power backend (see Fig. 4) with a bandwidth of 28 MHz centered at 8.45 GHz.

The measured SLL is below −19 dB and the difference with simulation is likely due to the residual misalignment of the BWG optics (M3 and M5). It is also worth to notice that Fig. 6 shows a slight asymmetry among the measured elevation and azimuth cuts due to a residual squint in the M1-M2 axes alignment. These SRT residual optics aberrations will be soon adjusted after a fine calibration of both the M3 position and the M2 look-up table by dedicated metrological measurements.

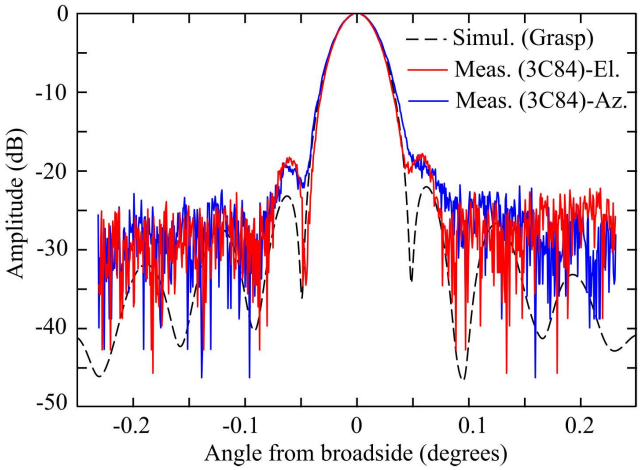

FIGURE 6. Normalized radiation pattern of the SDSA illuminated with the X-band feed horn at 8.45 GHz.

The measured half power beamwidth (HPBW) is in good agreement with the simulated one ($\theta_S = 0.039°$), as shown in Fig. 7 that reports the measured beam deformation ε with respect to the simulated HPBW at different elevation angles. ε is defined as:

$$\varepsilon = \sqrt{(\theta_{AZ} - \theta_S)^2 + (\theta_{EL} - \theta_S)^2} \tag{3}$$

where θ_{AZ} and θ_{EL} are, respectively, the HPBWs measured along the azimuth and elevation axis using the calibrator radio source 3C84. A quite stable beam deformation with respect to the elevation angle, with an average value of 0.002 degrees, is achieved thanks to the active optics of the SRT (see section 3.4.3 of [1]).

IV. DOWNLINK PERFORMANCE

The ratio antenna gain-to-system noise temperature (G/T_{sys}) is the primary figure of merit in the characterization of the downlink performance [19]. The antenna gain has been computed in the previous section, therefore we are left to estimate the system noise temperature that is defined as [20]:

$$T_{sys} = T_{Sky} + T_{Sp} + T_{rx} \tag{4}$$

with

$$T_{Sky} = T_{atm}\eta_S\left(1 - \exp\left(\frac{-\tau}{\sin\phi}\right)\right) + T_{CMB} \tag{5}$$

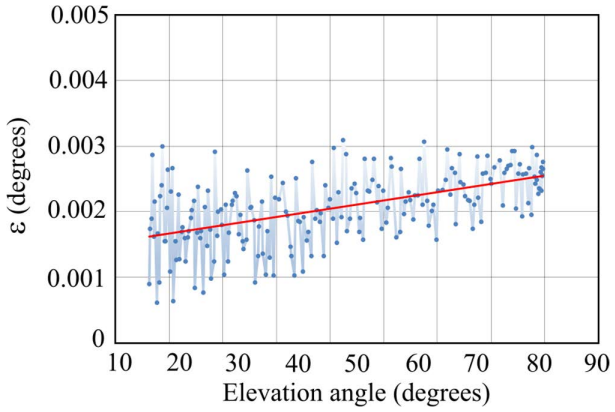

FIGURE 7. Measured beam deformation of the SDSA illuminated with the X-band feed horn at 8.45 GHz. The red line is the linear fit of measured data.

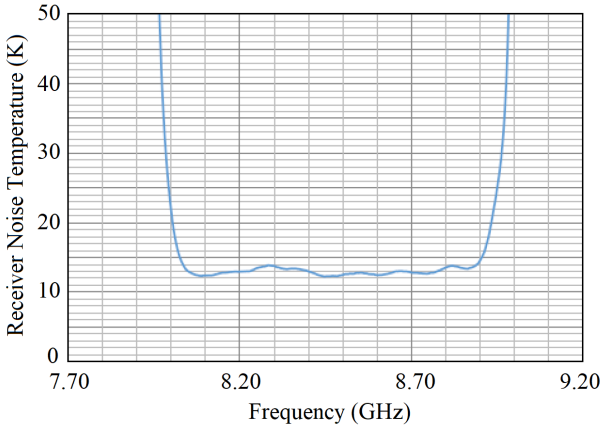

FIGURE 8. Measured noise temperature T_{rx} of the X-band receiver.

$$T_{Sp} = \eta_{M2}\,\eta_{M3}\,\eta_{M5}\,(1-\eta_{M1})\,T_{gnd} + \eta_{M3}\eta_{M5}\,(1-\eta_{M2})\,T_{sky} + \eta_{M5}\,(1-\eta_{M3})\,T_{gnd} + (1-\eta_{M5})T_{gnd} \quad (6)$$

where in

- T_{CMB} is the contribution from the cosmic background radiation (CMB), equal to 2.73 K.
- T_{atm} is the effective temperature of the atmosphere and τ is the zenithal sky opacity, both measured at 8.45 GHz using the *taumeter* available at the SRT site [21]: during our observations $\tau = 0.0077$ at elevation $\phi = 66°$ and $T_{atm} = 265$ K. The contribution of the first term of (5) is 2.61 K.
- T_{Sp} is the spillover temperature that includes the contribution of mirrors M1, M2, M3, and M5, given by (6), wherein η_{Mi} is the spillover efficiency of the mirror Mi computed using GRASP, and $T_{gnd} = 290$ K (η_{M1}, η_{M2}, η_{M3}, and η_{M5} are 0.998, 0.957, 0.996, and 0.953, respectively). Then the second term of (4) is estimated at $T_{Sp} = 15.3$ K.
- T_{rx} is the noise temperature generated by the active and passive microwave components of the receiver (see Fig. 4). The noise temperature T_{rx} added by this receiver has been measured at the NASA-JPL by using the Keysight PXA Spectrum Analyzer in noise figure analysis mode (see Fig. 8). The measured T_{rx} is about 13 K in the receiver frequency range.

In conclusion, the overall system noise temperature can be estimated at about 33.6 K, and the ratio antenna gain-to-system noise temperature at 57.1 dB/K.

The above estimates have been assessed by measurements of ratio G/T_{sys} at different elevation angles of the SDSA using the definition provided in [22] and, as a further validation, by separate measurements of the system temperature T_{sys} (see [23]).

Let P_n be the noise power at the backend total power (see Fig. 4) corresponding to the system noise temperature, i.e., in our case, the power from the cold sky in a 28 MHz bandwidth centered at 8.45 GHz. Let P_{st} be the additional noise power when the antenna is pointed towards a known radio source. Then, by measuring the following ratio

$$R = \frac{P_n + P_{st}}{P_n} \quad (7)$$

the value of G/T_{sys} can be determined using the formula [22]:

$$\frac{G}{T_{sys}} = \frac{8\pi k(R-1)}{\lambda^2 \Phi(f)} \quad (8)$$

wherein k (m^2 kg s^{-2} K^{-1}) is the Boltzmann's constant, λ (m) is the wavelength, and Φ (W m^{-2} Hz^{-1}) is the radiation flux-density of the selected known radio source as a function of the frequency f (Hz).

The ratio G/T_{sys} has been computed by selecting the calibrator radio source 3C147, whose flux value is stable at long and short timescales and it is well known and tabulated in the literature. Specifically, the flux value is evaluated to be 4.68±0.05 Jy at 8.45 GHz (1 Jy corresponds to 10^{-26} W m^{-2} Hz^{-1}) [24]. We have tracked the calibrator source from an elevation angle of 80° to the minimum elevation available for the SRT (about 6°), measuring both the power from the cold sky P_n and the additional power P_{st} from the calibrator. This allowed us to compute R using (7), and then the G/T_{sys} using (8).

On the other hand, an independent measurement of the system temperature T_{sys} has been provided relying on a calibrated noise source (or noise diode) that produces a known power per unit bandwidth. The noise diode has a known equivalent temperature, which is called calibration temperature T_{cal}, and the T_{sys} can be determined by the following expression [23]:

$$T_{sys} = \frac{P_n}{P_{cal} - P_n} T_{cal} \quad (9)$$

wherein the T_{cal} has been computed using the Y-Factor method [25] and P_{cal} is the noise power measured at the receiver output when the antenna is pointed towards the cold sky with the noise source switched on.

The measured T_{sys} is reported in Fig. 9, showing a good agreement with the estimate resulting from (4), i.e. 36.4 K at 66° elevation against 33.6 K.

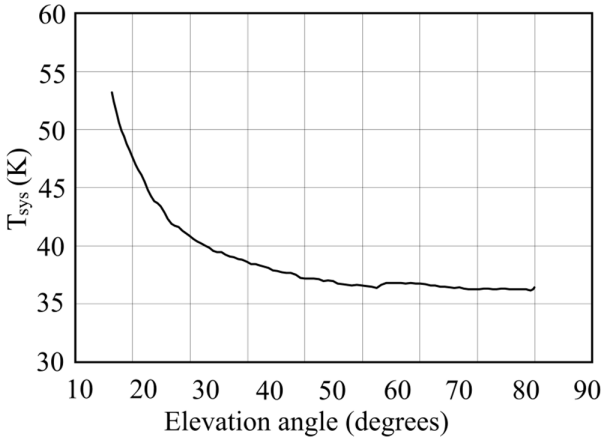

FIGURE 9. Measured T_{sys} of the SDSA at 8.45 GHz.

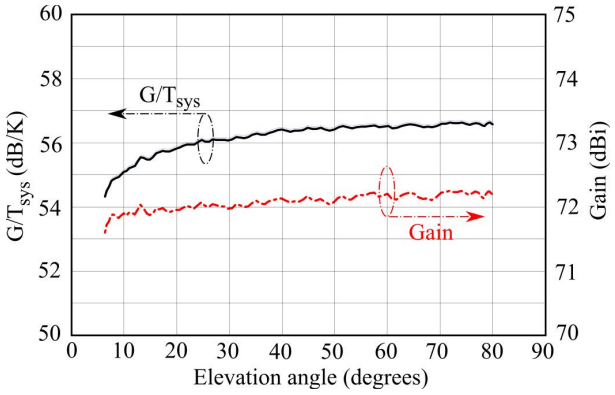

FIGURE 10. Measured G/T_{sys} and gain of the SDSA at 8.45 GHz.

In Fig. 10 we show the G/T_{sys} ratio, measured according to (7) and (8), for different elevation angles of the SRT. The measured value at the 66° elevation angle is 56.5 dB, 0.6 dB lower than the simulated estimate, mainly due to T_{sys} value underestimation of about 2.8 K (which contributes to about 0.35 dB).

Combining the results obtained by (8) and (9) we can derive an indirect measurement of the antenna Gain, which is also reported in Fig. 10. The measured gain is 72.1 dBi at 66° elevation angle, in good agreement with the estimates reported in Section III.

An important parameter for the characterization of the system performance is provided by the system equivalent flux density (SEFD). It represents the flux density, measured in W/(m^2 Hz), that a point source must have to produce an antenna temperature equal to the system temperature, and it is defined as [23]:

$$SEFD = \frac{2k}{A_{eff}} T_{sys} \tag{10}$$

wherein A_{eff} is the antenna effective area.

Using the definition (10), we can compute the sensitivity of the system ΔS, i.e. the minimum flux density that the system can detect:

$$\Delta S = \frac{SEFD}{\sqrt{BT}} \tag{11}$$

where B is the system frequency bandwidth and T is the integration time [26].

If we consider the measurement setup for the observation of the calibrator radio source 3C84 at 8.45 GHz, employed to compute the antenna beam pattern (see Fig. 6), with a bandwidth of 28 MHz and an integration time of 40 ms, we obtain $\Delta S = 0.0564$ Jy. Despite the radio source shows a variable flux density at long (months) timescales, we can infer a possible value in the range 26 ± 6 Jy [27], [28]. Considering this value, the signal-to-noise ratio is 26.5 dB $\pm$ 1 dB, which is consistent with the measurement shown in Fig. 6.

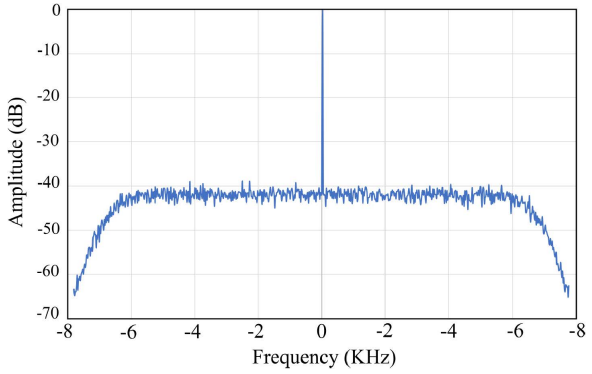

FIGURE 11. FFT spectrum of data received from the JUNO spacecraft.

TABLE 5. Estimated signal-to-noise ratio budget on JUNO.

Component	Block	Value
RF Power – Transmitter (dBm)	Spacecraft	44.4
Transmission Line Loss (dB)	Spacecraft	-0.9
Antenna Pointing Loss (dB)	Spacecraft	-0.9
Space Loss (dB)	Path	-290.7
Atmospheric Attenuation (dB)	Path	-0.2
Frequency (GHz)		8.404
Range (km)		966 E6
Antenna Gain (dBi) @30deg	Ground Station	72.15
Pointing Error (dB)	Ground Station	-0.2
System Noise Temperature (K) @30deg	Ground Station	39
Cryogenic receiver NF (K)	Ground Station	13
Sky temperature (K)		5.3
G/T (dB/K) @30deg	Ground Station	56.2
Signal power Density at receiver Input (dBHz)	Ground Station	-161.6
Receiver Noise Power (dBHz) (with BW = 1Hz)	Ground Station	-212.7
Telemetry carrier Suppression (dB)	Carrier Performance	-10.2
Signal-to-Noise Ratio		**40.9 dB**

V. TRACKING SESSION OF THE JUNO PROBE

Using the IFMS backend, on March 1st, 2021, at 11:35 UTC, we have received data from the Juno spacecraft with an antenna elevation of 30 degrees. The FFT spectrum shown in Fig. 11 is obtained by processing one second of these data. The open loop configuration was set in single channel mode

with a sampling frequency of 15625 Samples/s and 16 bits of quantization for both I and Q samples.

In Table 5, the downlink budget is reported and the estimated signal-to-noise ratio (about 41 dB) is consistent with the FFT spectrum reported in Fig. 11.

TABLE 6. Performance comparison of antennas for X-band deep space communication.

Agency	Location	D_A (m)	G/T_{sys} (dB/K)
Italian Space Agency (ASI)	**SDSA**	**64**	**56.5**
China National Space Agency (CNSA)	Jiamusi	66	53.3
	Kashi	35	49.0
	Neuquen	35	50.2
	Tianjing	70	55
European Space Agency (ESA)	New Norcia	35	55.5
	Cebreros	35	55.5
	Malargüe	35	55.5
Indian Space Research Organisation (ISRO)	Bylalu	32	47.0
Japan Aerospace Exploration Agency (JAXA)	Misasa	54	53.3
	Uchinoura	34	47.7
National Aeronautics and Space Administration (NASA)	Goldstone	34	54.2
	Canberra	34	54.2
	Madrid	34	54.2
	Goldstone	70	61.5
	Canberra	70	61.5
	Madrid	70	61.5
	Goldstone HEF	34	53.2
UK Space Agency (UKSA)	Goonhilly	32	45
	Goonhilly	30	55
Russian Space Agency (Roscosmos)	Bear Lakes	64	58.5
	Kalyazin	64	58.2

VI. CONCLUSION AND FUTURE PERSPECTIVES

The successful deployment of the SDSA has enabled the radio telescope to operate in the framework of the international deep space network. In this work we have presented the architecture and the performance of the X-band receiving system of the SDSA. Simulations, estimates, and measurements show that the SDSA can play a competitive role in the panorama of the X-band downlink systems for DSC, as apparent from Table 6 where we report a performance comparison of antennas for X-band DSC available in the world [29]. However, it should be noted that a direct comparison between the G/T_{sys} values in Table 6 is not fully consistent since they have been measured in different operating conditions, as discussed in [29].

The downlink capability of the SDSA provides a maximum value of the G/T_{sys} ratio equal to 56.5 dBi, which is achieved with the best alignment of the SRT BWG optics allowed by the current SRT optical configuration. Optimization of the SRT optics will be reached in the next few months after a fine calibration of both the BWG mirrors and the M2 look-up table by dedicated metrological measurements, aiming to reduce the SLL and increase the antenna gain.

TABLE 7. Possible downlink/uplink frequency plan of the SDSA program.

	Frequency (GHz)	Bandwidth (GHz)
X-Band Downlink	8.4 - 8.5	0.1
X-Band Uplink	7.145 – 7.235	0.09
K-Band Downlink	25.5 - 27	1.5
K-Band uplink	22.5 - 23.15	0.65
Ka-Band Downlink	31.8 - 32.3	0.5
Ka-Band uplink	34.2 - 34.7	0.5

At present, the capabilities of the SDSA are devoted to downlink communication. However, in the near future, ASI will evaluate the development of a transmitting system to enable uplink capabilities for deep space, near-earth, and lunar communication. Possibly, the BWG foci of the SRT devoted to space applications will be used to activate this functionality. In this context, the main future goal is to implement concurrent uplink and downlink transmission in X and Ka bands endowing the SDSA with a triple link X(uplink)/X(downlink), X(uplink)/Ka(downlink), and Ka(uplink)/Ka(downlink), according to the requirements of challenging radio science experiments. Simultaneous operation in the X and K band is also planned, mainly for near-earth and lunar communications. In Table 7 the possible operating frequency band for the above applications are reported.

REFERENCES

[1] P. Bolli *et al.*, "Sardinia radio telescope: General description, technical commissioning and first light," *J. Astronomical Instrum.*, vol. 4, nos. 3–4, Dec. 2015, Art. no. 1550008.
[2] I. Prandoni *et al.*, "The Sardinia radio telescope: From a technological project to a radio observatory," *Astron. Astrophys.*, vol. 608, no. A40, p. 26, 2017.
[3] G. Valente, G. Montisci, T. Pisanu, A. Navarrini, P. Marongiu, and G. A. Casula, "A compact L-band orthomode transducer for radio astronomical receivers at cryogenic temperature," *IEEE Trans. Microw. Theory Techn.*, vol. 63, no. 10, pp. 3218–3227, Oct. 2015.
[4] A. Melis *et al.*, "Sardinia Roach2-based digital architecture for radio astronomy (SARDARA)," *J. Astronomical Instrum.*, vol. 7, no. 1, Mar. 2018, Art. no. 1850004.
[5] G. Valente, T. Pisanu, A. Navarrini, P. Marongiu, A. Orfei, S. Mariotti, R. Nesti, J. Roda, A. Cattani, P. Bolli, and G. Montisci, "The coaxial L-P cryogenic receiver of the Sardinia radio telescope," *IEEE Access*, vol. 10, pp. 2631–2645, 2022.
[6] G. Muntoni, L. Schirru, G. Montisci, T. Pisanu, G. Valente, P. Ortu, R. Concu, A. Melis, E. Urru, A. Saba, F. Gaudiomonte, and G. Bianchi, "A space debris-dedicated channel for the P-band receiver of the Sardinia radio telescope: A detailed description and characterization," *Antennas Propag. Mag.*, vol. 62, no. 3, pp. 45–47, Jun. 2020.
[7] T. Pisanu, G. Muntoni, L. Schirru, P. Ortu, E. Urru, and G. Montisci, "Recent advances of the BIRALET system about space debris detection," *Aerospace*, vol. 8, no. 3, p. 86, Mar. 2021.
[8] *NASA Deep Space Network*. Accessed: Mar. 21, 2022. [Online]. Available: https://www.nasa.gov/directorates/heo/scan/services/networks/deep_space_network
[9] *Estrack Ground Stations*. Accessed: Mar. 21, 2022. [Online]. Available: https://www.esa.int/Enabling_Support/Operations/ESA_Ground_Stations/Estrack_ground_stations
[10] *Mars Rover Phones Home, Green Bank Telescope Answers*. Accessed: Mar. 21, 2022. [Online]. Available: https://greenbankobservatory.org/mars-rover-phones-home-green-bank-telescope-answers/
[11] G. Valente *et al.*, "Status of the radio receiver system of the Sardina radio telescope," *Proc. SPIE*, vol. 9914, Jul. 2006, Art. no. 991425.

[12] *Juno*. Accessed: Mar. 21, 2022. [Online]. Available: https://www.nasa.gov/mission_pages/juno/
[13] (Mar. 6, 2009). *European Cooperation for Space Standardization ECSS-E-ST-50-05C Rev.1—Radio Frequency and Modulation*. Accessed: Mar. 21, 2022. [Online]. Available: https://ecss.nl/standard/ecss-e-st-50-05c-rev-1-radio-frequency-and-modulation/
[14] F. Manshadi and R. Hartop, "Compound-taper feedhorn for the DSN 70-meter antennas," NASA JPL, California Inst. Technol., Pasadena, CA, USA, NASA-JPL TDA Prog. Rep. 42-90, Apr./Jun. 1987.
[15] E. Vassallo, R. Martin, R. Madde, M. Lanucara, P. Besso, P. Droll, G. Galtie, and J. De Vicente, "The European space agency's deep-space antennas," *Proc. IEEE*, vol. 95, no. 11, pp. 2111–2131, Nov. 2007.
[16] R. E. Collin, *Antennas and Radiowave Propagation*. New York, NY, USA: McGraw-Hill, 1985.
[17] J. Ruze, "Antenna tolerance theory—A review," *Proc. IEEE*, vol. 54, no. 4, pp. 633–640, Apr. 1966.
[18] M. Murgia *et al.*, "Sardinia radio telescope wide-band spectral-polarimetric observations of the galaxy cluster 3C 129," *Monthly Notices Roy. Astronomical Soc.*, vol. 461, no. 4, pp. 3516–3532, Oct. 2016.
[19] D. M. Pozar, *Microwave Engineering*. Hoboken, NJ, USA: Wiley, 2012.
[20] T. L. Wilson, K. Rohlfs, and S. Huttemeister, *Tools of Radio Astronomy*, 5th ed. Berlin, Germany: Springer-Verlag, 2009.
[21] F. Buffa, P. Bolli, G. Sanna, and G. Serra, "An atmosphere monitoring system for the Sardinia radio telescope," *Meas. Sci. Technol.*, vol. 28, no. 1, Nov. 2016, Art. no. 014004.
[22] *Determination of the G/T Ratio for Earth Stations Operating in the Fixed-Satellite Service*, document Rec. ITU-R S.733-2, International Communication Union. Accessed: Mar. 21, 2022. [Online]. Available: https://www.itu.int/dms_pubrec/itu-r/rec/s/R-REC-S.733-2-200001-I!!PDF-E.pdf
[23] J. M. Marr, R. L. Snell, and S. E. Kurtz, *Fundamentals of Radio Astronomy*. Boca Raton, FL, USA: CRC Press, Taylor & Francis, 2016.
[24] R. A. Perley and B. J. Butler, "An accurate flux density scale from 50 MHz to 50 GHz," *Astrophysical J. Suppl. Ser.*, vol. 230, no. 1, p. 18, May 2017.
[25] Rohde & Schwarz. *The Y Factor Technique for Noise Figure Measurements. Application Note*, Accessed: Mar. 21, 2022. [Online]. Available: https://scdn.rohde-schwarz.com/ur/pws/dl_downloads/dl_application/application_notes/1ma178/1MA178_4e_NoiseFigure.pdf
[26] N. Skou and D. Le Vine, *Microwave Radiometer Systems*, 2nd ed. Norwood, MA, USA: Artech House, 2006.
[27] R. Ricci *et al.*, "A first extended catalogue of pointing/focus calibrators for the Sardinia radio telescope," INAF IRA, Bologna, Italy, Internal Rep. INAF IRA 496/16, Jul. 2016. Accessed: Mar. 21, 2022. [Online]. Available: http://www.ira.inaf.it/Library/rapp-int/496-16.pdf
[28] S. Britzen, C. Fendt, M. Zajaček, F. Jaron, I. Pashchenko, M. F. Aller, and H. D. Aller, "3C 84: Observational evidence for precession and a possible relation to TeV emission," *Galaxies*, vol. 7, no. 3, p. 72, Aug. 2019.
[29] Mars Communications Architecture. (Feb. 22, 2022). *Report of the Interagency Operations Advisory Group Mars and Beyond Communications Architecture Working Group*. Accessed: Mar. 21, 2022. [Online]. Available: https://www.ioag.org/Public%20Documents/MBC%20architecture%20report%20final%20version%20PDF.pdf

GIUSEPPE VALENTE received the M.S. degree in electronic engineering and the Ph.D. degree in electronic engineering and computer science from the University of Cagliari, Cagliari, Italy, in 2007 and 2016, respectively. From 2009 to 2016, he was with the National Institute for Astrophysics (INAF), Cagliari Astronomy Observatory, Cagliari, where he worked on the development of the receivers for Sardinia Radio Telescope. Since 2016, he has been a Researcher at Italian Space Agency. He is currently a Project Scientist of Sardinia Deep Space Antenna and RF Systems. His research interests include electromagnetic design for deep-space applications, in particular low noise microwave systems and radiofrequency calibration instrumentation.

MARIA NOEMI IACOLINA received the M.S. degree in physics and the Ph.D. degree in astrophysics and nuclear physics from Cagliari University. She worked at the INAF—Observatory of Cagliari, from 2010 to 2016, where she actively participated to the astronomical validation of the Sardinia Radio Telescope, also producing astronomical software devoted to the planning and data reduction of astronomical observations. Since 2016, she has been a Researcher with Italian Space Agency, where she works for the Sardinia Deep Space Antenna as a Project Scientist of the Program, mainly focusing on calibrations and space scientific applications.

RICCARDO GHIANI received the bachelor's degree in electronic engineering from Cagliari University, Cagliari, Italy, in 2015, with a thesis involving the design of RF components. After a short experience with the Electromagnetic Group, Cagliari University, since 2019, he has been collaborating with Italian Space Agency (ASI) for the Sardinia Deep Space Antenna. He is currently working on signal analysis and evaluation and measurement of SDSA performance.

ANDREA SABA received the M.S. degree in computer science and the Ph.D. degree in mathematics and computer science from the University of Cagliari, Cagliari, Italy, in 2006 and 2009, respectively. He has coauthored articles in international journals on *Theoretical Computer Science*. From 2011 to 2018, he was with the National Institute for Astrophysics (INAF), Cagliari Astronomy Observatory, Cagliari, where he worked on the development of the INAF node at the VAMDC consortium, on the development of a photogrammetry simulator for the Sardinia Radio Telescope and to the firmware and software development for radio astronomy and space applications. Since 2019, he has been a Technologist at Italian Space Agency and he is currently the Project Manager of Sardinia Deep Space Antenna Networking and SW Development. His research interests include firmware and software development for space applications.

GIAMPAOLO SERRA received the M.S. degree in electronic engineering and the Ph.D. degree in electronic engineering and computer science from the University of Cagliari, Italy, in 2004 and 2008, respectively. After one year working with the Department of Electrical and Electronic Engineering, University of Cagliari, he joined the National Institute for Astrophysics, Astronomical Observatory of Cagliari for ten years. He worked there first in the development of the microwave holography system for the Sardinia Radio Telescope. Subsequently, he contributed toward the commissioning of the SRT. In particular, he was involved in the design of the telescope metrology system, of which became then the Coordinator, and in the Radio Frequency Interference. He performed holographic measurements at Medicina telescope, in 2009 and 2010, and at SRT, in 2016, 2017, and 2018, mapping the surface deformations of both telescopes primary reflector. Moreover, he performed routinely RFI monitoring at SRT site and two RFI surveys at Noto telescope, in 2015 and 2016. Since 2019, he has been working with Italian Space Agency in the development of the deep space downlink capability of the SRT, a.k.a. SDSA. He is also a Project Manager responsible for the SDSA metrology and operations. He is collaborating with INAF to upgrade the SRT metrology system in order to improve the antenna pointing and main reflector surface alignment accuracies. His research interests include microwave holography, metrology and control of large reflector antennas performances, RFI, and atmosphere monitoring.

ENRICO URRU received the M.S. degree in electronic engineering from the University of Cagliari, Cagliari, Italy, in 2007. From 2009 to 2012, he worked in private companies in the defense sector. From 2013 to 2020, he was with the National Institute for Astrophysics (INAF), Cagliari Astronomy Observatory, Cagliari, where he worked on the development and integration of the receivers and on the metrology activities for Sardinia Radio Telescope and on the SST European project for Space debris monitoring. Since June 2020, he has been a Technologist at Italian Space Agency (ASI) and he is currently involved in the Sardinia Deep Space Antenna Development and Operations. His research interests include ground segment engineering and on the digital backend development and setup for deep-space applications.

GIORGIO MONTISCI (Senior Member, IEEE) received the M.S. degree in electronic engineering and the Ph.D. degree in electronic engineering and computer science from the University of Cagliari, Cagliari, Italy, in 1997 and 2000, respectively. Since February 2022, he has been a Full Professor in electromagnetic fields with the University of Cagliari, teaching courses in electromagnetics and microwave engineering. He has authored or coauthored 75 articles in international journals. His current research interests include the analysis and design of waveguide slot arrays, RFID antennas, wearable antennas, numerical methods in electromagnetics, and microwave circuits and systems. He is an Associate Editor of IEEE Access, *IET Microwaves, Antennas & Propagation*, *IET Electronics Letters*, and an Academic Editor of the *International Journal of Antennas and Propagation*. He was awarded the IEEE Access Outstanding Associate Editor of 2020.

SARA MULAS received the M.S. degree in physics from the University of Cagliari, with a thesis on the spectropolarimetric studies of Supernova Remnants with the Effelsberg and the Sardinia Radio Telescope and the Ph.D. degree in physics astrophysics from the University of Cagliari, in 2019. She was a recipient of the Research Grant University of Cagliari-Italian Space Agency in collaboration with the Italian National Institute for Astrophysics. Her work is mainly focused on investigating the scientific requirements to perform a radio science experiment with a deep space antenna and studying the radio sun with the Sardinia radio telescope in single-dish imaging modality aiming to space weather applications.

SAMI W. ASMAR is currently the General Secretary of the Consultative Committee for Space Data Systems (CCSDS) and its NASA Chief Delegate. He is also the Manager of Strategic Partnerships at the Interplanetary Network Directorate, NASAs Jet Propulsion Laboratory, California Institute of Technology. He is also the author of the 2022 book *Radio Science Techniques for Deep Space Exploration* (John Wiley & Sons), and a Radio Science co-investigator on many U.S. and European planetary missions.

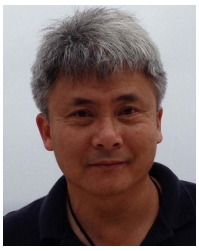

TIMOTHY T. PHAM is currently the Chief System Engineer of the NASA Deep Space Network. His research interests include system engineering and system development. Besides DSN system engineering work, he also supports the CCSDS activities in cross support transfer services and the ground system development at Morehead State University. He has published several papers on antenna arraying, spacecraft tracking, system modeling, and performance analysis. He coauthored the book *Antenna Arraying Techniques in the Deep Space Network*. He was a recipient of the NASA Exceptional Service Medal, NASA Exceptional Achievement Medal, several NASA New Technology and Space Act Awards, and the IARIA Fellow.

JAVIER DE VICENTE has been a Ground Stations Systems Engineer at ESA, since 2000. He has been a Technical Officer for many studies and subsystem developments and the Project Manager for ground station deployments. He is currently responsible for the ESA Delta DOR correlator and the implementation of the Radio Science capability in ESA Deep Space Antennas.

SALVATORE VIVIANO is currently pursuing the Graduate degree in aeronautical engineering with the School of Aerospace Engineering, Sapienza University of Rome. He is the Manager of Sardinia Deep Space Antenna. He has about 35 years of experience in aerospace sector, working for several private companies and public administrations. His main technical and managerial experiences include flight dynamics, control centers, operations for S/C and constellation, and satellite communication and navigation, in particular managing the development of GPS signal in space and differential applications in many areas, EGNOS applications for civil aviation and contributing in Galileo system development and regulation for its governmental use.